

YALE PEABODY MUSEUM

P.O. BOX 208118 | NEW HAVEN CT 06520-8118 USA | PEABODY.YALE. EDU

JOURNAL OF MARINE RESEARCH

The *Journal of Marine Research*, one of the oldest journals in American marine science, published important peer-reviewed original research on a broad array of topics in physical, biological, and chemical oceanography vital to the academic oceanographic community in the long and rich tradition of the Sears Foundation for Marine Research at Yale University.

An archive of all issues from 1937 to 2021 (Volume 1–79) are available through EliScholar, a digital platform for scholarly publishing provided by Yale University Library at <https://elischolar.library.yale.edu/>.

Requests for permission to clear rights for use of this content should be directed to the authors, their estates, or other representatives. The *Journal of Marine Research* has no contact information beyond the affiliations listed in the published articles. We ask that you provide attribution to the *Journal of Marine Research*.

Yale University provides access to these materials for educational and research purposes only. Copyright or other proprietary rights to content contained in this document may be held by individuals or entities other than, or in addition to, Yale University. You are solely responsible for determining the ownership of the copyright, and for obtaining permission for your intended use. Yale University makes no warranty that your distribution, reproduction, or other use of these materials will not infringe the rights of third parties.



This work is licensed under a Creative Commons Attribution-NonCommercial-ShareAlike 4.0 International License.
<https://creativecommons.org/licenses/by-nc-sa/4.0/>



Stability of the global ocean circulation: The connection of equilibria within a hierarchy of models

by **Henk A. Dijkstra^{1,2}** and **Wilbert Weijer³**

ABSTRACT

We address the problem of the multiple equilibria of the thermohaline circulation in a hierarchy of models. The understanding of the relation between bifurcation diagrams of box models, two-dimensional models and those of a global ocean general circulation model, is facilitated through analysis of the equilibrium solutions of a three-dimensional Atlantic-like sector model with an open southern channel. Using this configuration, the subtle effects of the wind-stress field, the effects of continental asymmetry and the asymmetry in the surface freshwater flux can be systematically studied. The results clarify why there is an asymmetric Atlantic circulation under a near equatorially-symmetric buoyancy forcing. They also lead to an explanation of the hysteresis regime that is found in models of the global ocean circulation. Both explanations are crucial elements to understanding the role of the ocean in past and future climate changes.

1. Introduction

The behavior of the thermohaline circulation under changes in external forcing conditions is a subject of intense study. There is discussion on the precise definition of the thermohaline circulation (Wunsch, 2002; Rahmstorf, 2003) but in many studies focusing on transitions due to changes in forcing conditions, it is viewed as that part of the ocean circulation which differs from the pure wind-driven ocean circulation due to the presence of fluxes of heat- and freshwater at the ocean-atmosphere surface. This circulation can be represented in coarse-resolution GCMs having a simplified wind-driven component where the mixing effect of small-scale phenomena is represented as downgradient diffusion. However, even within this framework there is confusion on the mechanisms maintaining the circulation and causing transition (Marotzke, 2000).

Near the equator, there is a strong warming of the surface waters and those at higher latitudes are cooled. At subtropical latitudes there is strong evaporation whereas at high latitudes precipitation is larger than evaporation. A characteristic of both zonally averaged, annual-mean heat- and freshwater flux is their near-equatorial symmetry

1. Institute for Marine and Atmospheric Research Utrecht, Department of Physics and Astronomy, Utrecht University, Utrecht, The Netherlands.

2. Department of Atmospheric Science, Colorado State University, Fort Collins, Colorado 80523, U.S.A. *email: dijkstra@atmos.colostate.edu*

3. Scripps Institution of Oceanography, University of California, La Jolla, California 92093, U.S.A.

(Oberhuber, 1988; Zaucker *et al.*, 1994; Josey *et al.*, 1999). Both salinity and temperature affect the density and consequently a large-scale flow is driven by the horizontal temperature and salinity gradients, if they extend over a substantial depth in the ocean. As a first guess of the circulation, one would propose the existence of an equator-to-pole circulation in each hemisphere, with either upwelling or downwelling at the equator. The latter would depend on whether salinity or temperature dominates in the density field (Welander, 1986).

This is not the case: the observed flow in the Atlantic is pole-to-pole and strongly equatorially asymmetric. There is a net sinking of deep water of about 15 Sv in the North Atlantic that is associated with the formation of North Atlantic Deep Water (NADW). The NADW can be traced down to 30S in the South Atlantic and connects more southward to water masses from the Southern Ocean. The northward heat transport of this single pole-to-pole cell is positive at every latitude north of 30S (Ganachaud and Wunsch, 2000). Also the zonally averaged circulation in the Pacific is asymmetric consisting of two vertically stacked overturning cells with inflow from the south at the bottom and the surface and outflow at mid-depths (Schmitz, 1995). A central problem is, therefore, why the thermohaline circulation in both the Atlantic and Pacific is so asymmetric under fairly equatorially symmetric buoyancy-forcing conditions.

A recent bifurcation study of the overturning circulation in the Atlantic Ocean (Dijkstra *et al.*, 2003) has confirmed (within a 3D model context) the idea that asymmetric circulation patterns may arise under symmetric forcing conditions (Bryan, 1986). It also showed that natural asymmetries in the geometrical properties of the Atlantic, as well as in the forcing conditions, lead to a strong preference of a northern sinking circulation in this basin.

The sensitivity of the global ocean circulation to buoyancy input into the North Atlantic has been investigated by adding freshwater at a very slow rate such that quasi-steady states are monitored in time (Rahmstorf, 1995; Prange *et al.*, 2002). In this way, a first impression of the stable equilibria of the global ocean circulation can be obtained (Rahmstorf, 2000). In a global ocean general circulation model (OGCM) that is coupled to a zeroth-order atmosphere model, it is found that when this freshwater input is strong enough, the ocean circulation collapses as the northern overturning strongly decreases. When the freshwater forcing is reversed from the collapsed state, hysteresis behavior occurs because the off-state can be maintained under substantial positive freshwater-flux anomalies. As the anomalous freshwater input greatly influences the equatorial asymmetry of the forcing, the dynamics of the existence of the hysteresis regime and the problem of the asymmetric overturning circulation in the Atlantic may be closely linked.

Recently, it has become possible to compute bifurcation diagrams for global low-resolution OGCMs (Weijer and Dijkstra, 2003). These diagrams map the equilibria of the system under consideration (stable and unstable) when crucial parameters are varied. To connect to quasi-equilibrium studies where in a transient integration a regional freshwater flux anomaly is imposed (Rahmstorf, 1995), explicit bifurcation diagrams were computed

under different (steady) freshwater flux patterns. The hysteresis regime was found, indicating a regime of multiple equilibria where both northern and southern overturning states for the Atlantic exist, with relatively minor changes in the rest of the world ocean. Combining the results of the Atlantic model in Dijkstra *et al.* (2003) and those of the global model may provide the key in determining the connection between the existence of the asymmetric Atlantic circulation and the existence of the hysteresis regime.

In this paper, we focus on understanding this connection and investigate the bifurcation diagrams for a hierarchy of models. On the low end of the model hierarchy are simple box models (Stommel, 1961; Rooth, 1982; Welander, 1986) and on the other end is a global ocean model with full continental geometry and bathymetry. It turns out that the bifurcation diagrams for the Atlantic configuration studied in Dijkstra *et al.* (2003) form an excellent bridge of the results over the model hierarchy; most of the results presented here will be for that configuration. By going down the hierarchy, the link between asymmetric properties of the Atlantic circulation and the hysteresis regime is clarified. By arriving at the box model level, the results identify the box model that best represents the dynamics of the Atlantic thermohaline circulation.

2. Hysteresis in a global ocean-atmosphere model

In Weijer and Dijkstra (2003), a global ocean model was coupled to an energy balance model of the atmosphere. The governing equations of the ocean model are the hydrostatic, primitive equations in spherical coordinates on a domain that includes full continental geometry as well as bottom topography. The horizontal resolution is about 4° , with a 96×38 grid on a domain $[0, 360] \times [-85.5, 85.5]$. The grid has 12 levels in the vertical and is nonequidistant with the most upper (lowest) layer having a thickness of 50 m (1000 m), respectively.

Starting from the trivial state (at zero solar forcing, no freshwater flux and no wind-stress) first an equilibrium state is determined under the annual-mean wind stress as in Trenberth *et al.* (1989), an analytical form of the solar forcing and the Levitus surface salinity distribution (Levitus *et al.*, 1994). The freshwater flux of this reference solution is diagnosed and subsequently used as part of the surface buoyancy forcing. Although the diagnosed freshwater differs substantially from the observed annual mean field, there is reasonable agreement with the diagnosed fluxes in other OGCMs (Weaver and Hughes, 1996). Next, a steady perturbation pattern in the freshwater flux over a relatively small domain in the North Atlantic ($(\phi, \theta) \in [300, 336] \times [54, 66]$) is applied.

Bifurcation diagrams were computed in two parameters γ and γ_p . The dimensionless parameter γ indicates the strength of the diagnosed freshwater flux where $\gamma = 1$ is compatible with the freshwater flux needed to maintain the Levitus surface salinity field. The parameter γ_p is the amplitude (in Sv) of the anomalous North Atlantic perturbation in the freshwater flux. The emergence of the multiple equilibrium regime with changing freshwater flux can be seen by plotting several bifurcation diagrams in γ for several fixed values of γ_p (Fig. 1a).

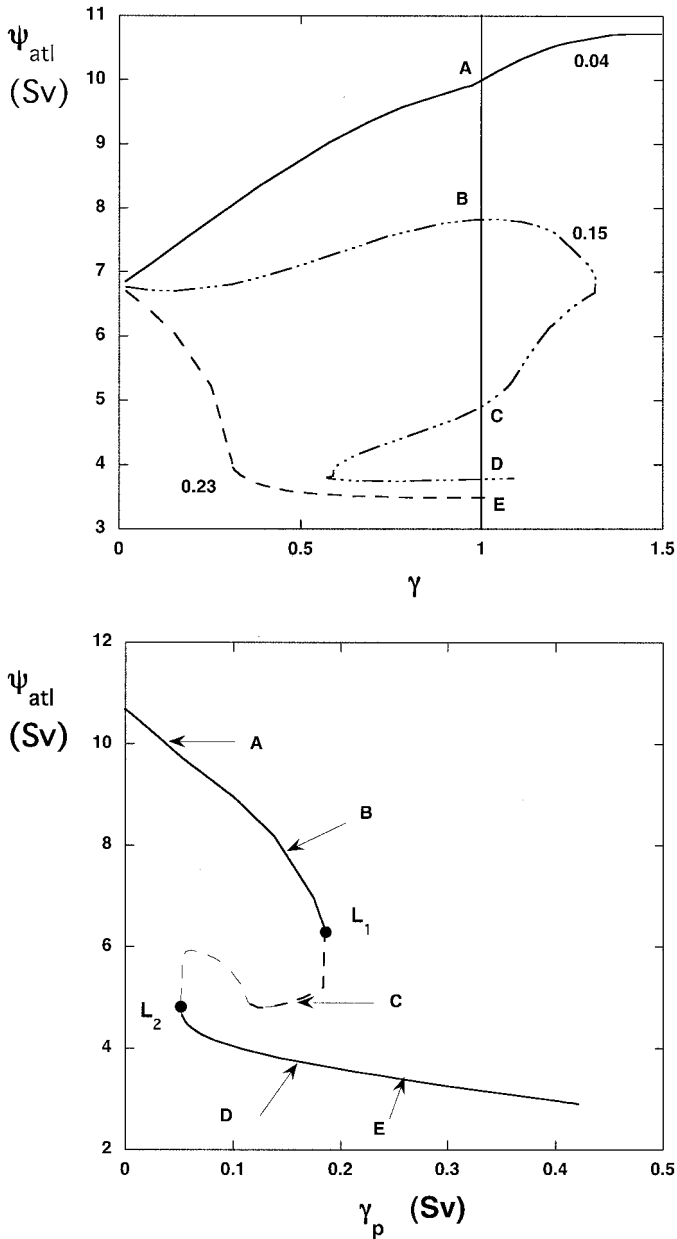


Figure 1. (a) Bifurcation diagrams of the global ocean model for several values of γ_p , as curves of the maximum Atlantic meridional overturning versus the strength of the diagnosed freshwater flux γ . Stable states are indicated by drawn curves and dashed curves indicate unstable states. (b) Hysteresis bifurcation diagram in γ_p for fixed $\gamma = 1$.

For $\gamma_p = 0.04$ Sv, the overturning increases with γ , while no multiple equilibria occur. For $\gamma_p = 0.15$ Sv, however, two saddle-node bifurcations appear and the collapsed solution is the only solution beyond $\gamma = 1.25$. For $\gamma_p = 0.23$ Sv, the overturning decreases monotonically with γ along the southern sinking branch. As γ changes only the amplitude of the diagnosed freshwater flux, these results demonstrate the dominant role of the spatial pattern of the freshwater flux, controlled by γ_p , in the existence of the multiple equilibrium regime.

When γ_p is changed for fixed $\gamma = 1$, a hysteresis behavior is found (Fig. 1b) similar to results of quasi-equilibrium simulations performed with OGCMs and climate models. It is mostly the Atlantic circulation that changes drastically along this diagram; the Pacific and Indian Ocean circulations are less affected. The saddle-node bifurcations exactly bound the regime of multiple equilibria of these flows. In this model configuration, one needs to increase the amplitude of the freshwater flux perturbation beyond $\gamma_p = 0.052$ Sv to be into the multiple equilibria regime and hence for the existence of a possible collapse of the Atlantic overturning circulation. For values smaller than $\gamma_p = 0.18$ Sv, only the collapsed state exists.

The diagrams in Figure 1 show two issues that are important for the discussions below. First issue is that the Atlantic overturning increases with γ for the northern sinking state (γ_p small). Similarly, the strength of the southern overturning state (not shown) increases with γ (γ_p large). Second, hysteresis behavior only occurs when the freshwater flux is sufficiently asymmetric (γ_p below a certain negative value).

3. Equilibria of an Atlantic THC model

As the dynamical changes to the freshwater input seem to have effect mainly on the Atlantic circulation, it makes sense to use an ‘Atlantic only’ model. Such a configuration was used in Dijkstra *et al.* (2003) to investigate the bifurcation diagrams with respect to the strength of the freshwater forcing, the latter having a fixed spatial pattern. The structure of steady states of the thermohaline circulation was considered in a double-hemispheric domain for a coupled three-dimensional ocean-atmosphere model. Both an equatorially symmetric situation (referred to as the ‘closed’ configuration) and a situation in which an open southern channel was represented (referred to as the ‘open’ configuration) were considered. The presence of a representation of the Antarctic Circumpolar Current gives a strong preference for the northern sinking solution. When winds are absent, the southern sinking branch becomes a closed curve and solutions exist for only a small range of freshwater flux strengths. The effect of the presence of zonally averaged winds is to shrink the isolated branch into a single point (isola) and make it disappear, leading to only a single branch of equilibria with northern sinking. In this section, we use the ‘open’ version of the model with a southern channel and study the effects of anomalous freshwater input, similar to that used in the global model.

The model is actually derived from the global ocean model of the previous section. The equations are solved on a sector domain, with $\phi_W = 282$, $\phi_E = 354$, $\theta_S = -70$ and

$\theta_N = 70$. At the east-west boundaries, a zonal sector of 4° is covered by land, except for a 16° latitude band at the southern boundary. The basin has a flat bottom, its depth D is 4 km and periodic boundary conditions are applied in zonal direction within the southern channel. As in Dijkstra *et al.* (2003), a grid of 4° horizontal resolution, 16 vertical equidistant layers (a grid of $18 \times 35 \times 16$) is applied. The methodology to compute the steady solution branches is presented in Dijkstra *et al.* (2003) and will not be repeated here.

a. Basic bifurcation diagram: No wind

The standard freshwater flux pattern used (F_S^b) is plotted as the drawn curve in Figure 2a. A bifurcation diagram for the same standard parameter values (no windstress) as in Table 1 of Dijkstra *et al.* (2003) is shown in Figure 2b. The maximum of the northward meridional overturning streamfunction (in Sv) is plotted versus γ where γF_0 ($F_0 = 3.9 \times 10^{-6} \text{ m s}^{-1}$) is the dimensional freshwater-flux strength. Note that a value $F_0 = 10^{-6} \text{ m s}^{-1}$ corresponds to an actual value of $P - E = 74 \text{ mm/month}$. This bifurcation diagram is the same as that in Figure 4 of Dijkstra *et al.* (2003), except that there the absolute maximum streamfunction and only the part near the pitchfork bifurcation of the ‘closed’ case was plotted. Hence, the shape of the isolated branch (which represents the southern sinking solutions) is different.

In quasi-equilibrium simulations with ocean models, a freshwater anomaly is applied to the surface layer. To close the salt balance, either salt is added homogeneously over the remainder of the domain, or it is added to a remote region. In a transient simulation, the response to this freshwater anomaly is monitored. To mimic this in the Atlantic model, we consider the equilibrium response to parametric variation of the freshwater flux pattern, i.e.,

$$F_S = \gamma F_0 F_S^b + \gamma_p F_0 F_S^p - Q \quad (1a)$$

$$F_S^p(\theta) = -\exp\left[\frac{-(\theta - \theta_*)^2}{a_*^2}\right]. \quad (1b)$$

When changing γ_p , one has to take care that the salt balance is closed, i.e., the offset Q has to be adapted such that

$$\frac{1}{|S|} \int_S F_0 (\gamma F_S^b(\theta) + \gamma_p F_S^p(\theta)) r_0^2 \cos \theta d\theta d\phi - Q = 0. \quad (2)$$

We take $\theta_* = 20^\circ$ and $a_* = 5^\circ$ such that the perturbation is centered around the maximum of the freshwater flux F_S^b . An example of the total freshwater flux for $\gamma_p = 0.2$ is shown as the dash-dotted curve in Figure 2a.

The bifurcation diagrams for $\gamma_p = 0.2$ and $\gamma_p = 0.6$ are plotted in Figure 3. As soon as the freshwater flux becomes asymmetric, the isolated branch connects up with the northern sinking branch. The shape of the freshwater flux, with net input of freshwater in the

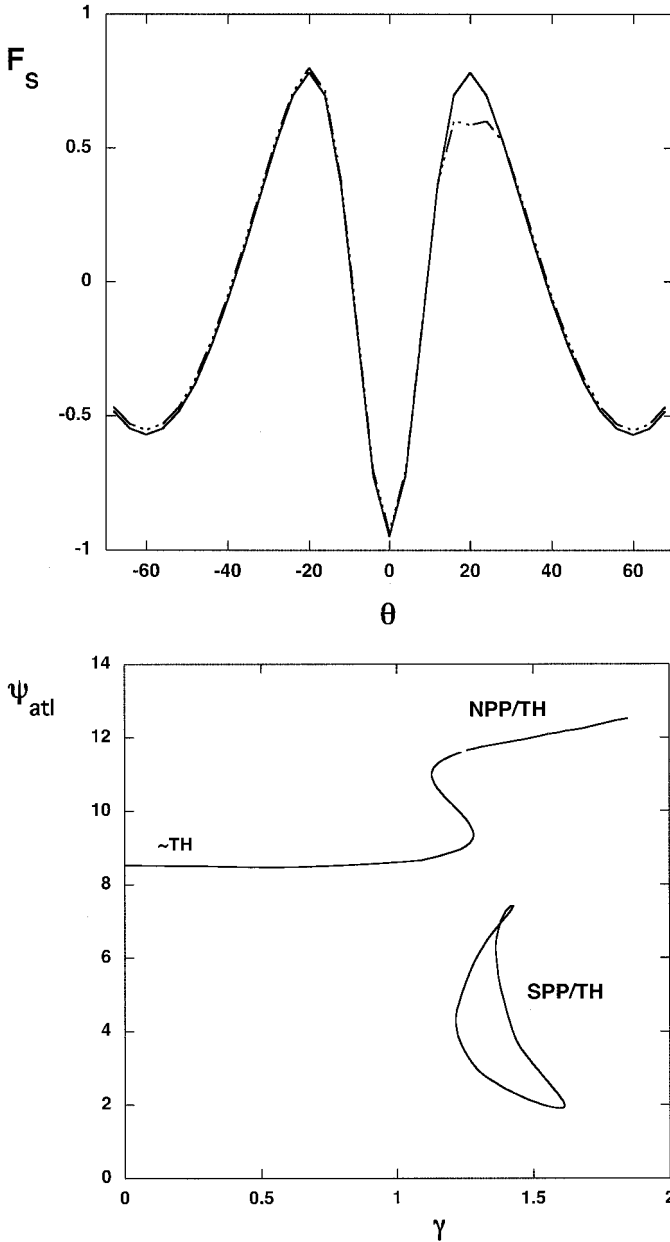


Figure 2. (a) Patterns of the freshwater flux used for the Atlantic model. The drawn curve is the standard equatorially symmetric freshwater flux; the dash-dotted curve is the same freshwater flux with a component F_s^p (see (1)) added with $\gamma_p = 0.2$. (b) Bifurcation diagram for the standard 'open' case. The maximum northward overturning is plotted versus the strength of the freshwater flux γ . No indication of stability of the branches is given.

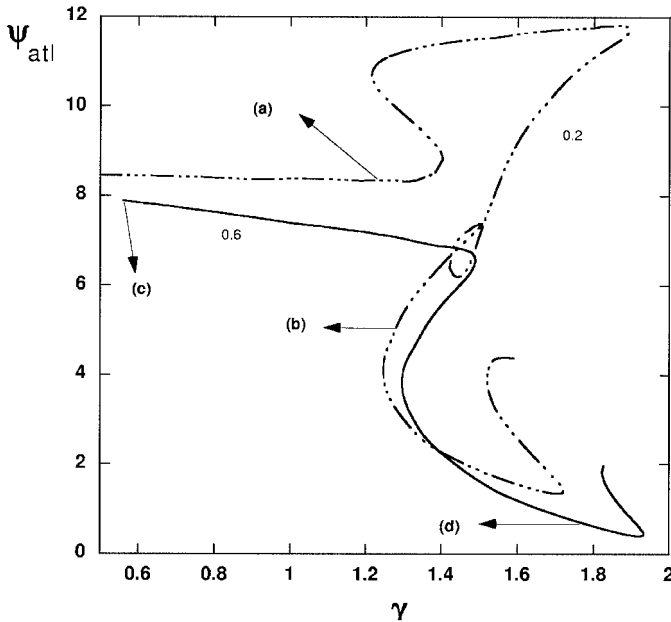


Figure 3. Bifurcation diagrams for two values of γ_p , i.e., $\gamma_p = 0.2$ (dash-dotted) and $\gamma_p = 0.6$ (drawn). The line style does not provide indications of stability. Solutions for the meridional streamfunction at labeled locations are shown in Figure 4.

northern part of domain, induces a preference for the southern sinking solution. The diagram for $\gamma_p = 0.2$ is fairly complicated with a small region where there exist five(!) steady states and a substantially larger region with three steady states.

Solutions for the meridional overturning streamfunction are shown in Figure 4 at selected locations in Figure 3. A continuous deformation from the northern sinking branch (NPP/TH) to the southern sinking branch (SPP/TH) is seen from the meridional overturning streamfunctions in Figure 4a–b. For $\gamma_p = 0.6$, the equatorial asymmetry due to anomalous freshwater flux has become so strong that there is already a preference for southern sinking at small γ (Fig. 4c). A strong northern sinking branch has disappeared and hysteresis appears over a region near $\gamma = 1.3$. Hence, in a way the asymmetry in the freshwater flux opposes the preference for the northern sinking branch, the latter is preferred by all other asymmetric effects. A strong southern sinking cell occurs at large values of γ (Fig. 4d).

b. The effect of the wind stress

It was found in Dijkstra *et al.* (2003) that the isolated branch in Figure 2b did disappear when the effect of the zonally-averaged wind stress (taken from Trenberth *et al.* (1989)) was taken into account. The wind stress is strong enough to prohibit the existence of the

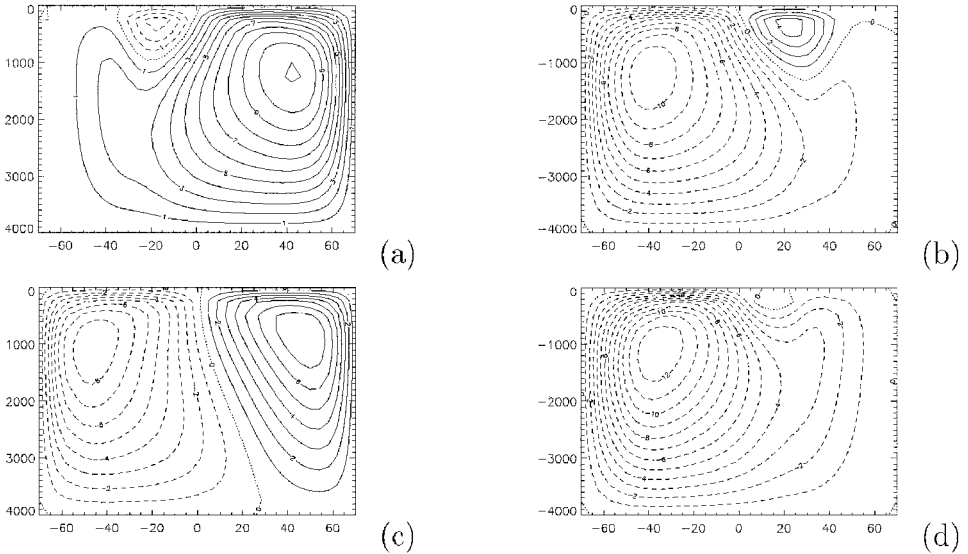


Figure 4. Patterns of the meridional overturning at several labeled locations in Figure 3. (a) $\gamma = 1.24$, $\Psi_{min} = -3.55$, $\Psi_{max} = 11.1$, (b) $\gamma = 1.28$, $\Psi_{min} = -10.8$, $\Psi_{max} = 4.46$, (c) $\gamma = 0.52$, $\Psi_{min} = -8.86$, $\Psi_{max} = 7.92$ and (d) $\gamma = 1.69$, $\Psi_{min} = -12.8$, $\Psi_{max} = 0.91$. Contour interval is 1 Sv.

southern sinking branch due to the northward Ekman transport in the upper layers of the ocean. The bifurcation diagram with $\tau_0 = 0.1$ and $\gamma_p = 0.0$ is shown as the solid curve in Figure 5a. There are only small regions in γ , the intervals $\gamma \in [1.029, 1.040]$ and $\gamma \in [1.529, 1.804]$, where multiple equilibria exist.

Solutions for the meridional overturning streamfunction are shown in Figure 6 at selected locations in Figure 5a. Along the branch for $\gamma_p = 0$, there are only northern overturning solutions because the continental asymmetry as well as the Ekman transport prohibit the existence of a southern sinking solution. The strength of the northern overturning increases with γ indicating that salinity helps in driving the flow (giving rise to real thermohaline driven circulation) and that the salt-advection feedback is actively involved to maintain the flow. In the present case with wind-stress forcing, there is a smooth transition between the branches for $\gamma_p = 0.0$ and $\gamma_p = 1.0$, not involving connections with isolated states. For $\gamma_p = 1.0$, there is already a preference for the southern sinking solution at small γ (Fig. 6c). The effect of the salt-advection feedback leads to a stronger southern sinking solution at large γ (Fig. 6d).

The branches in Figure 5a clearly resemble those of the global model in Figure 1a, except for the small hysteresis regimes at small γ , and the small multiple equilibria regime at larger γ . On the TH/SPP branch, a similar small hysteresis occurs for $\gamma_p = 1.0$ as on the TH/NPP branch for $\gamma_p = 0.0$. Since both branches are originally symmetry related, the mechanism of the occurrence of this small hysteresis is similar and related to the

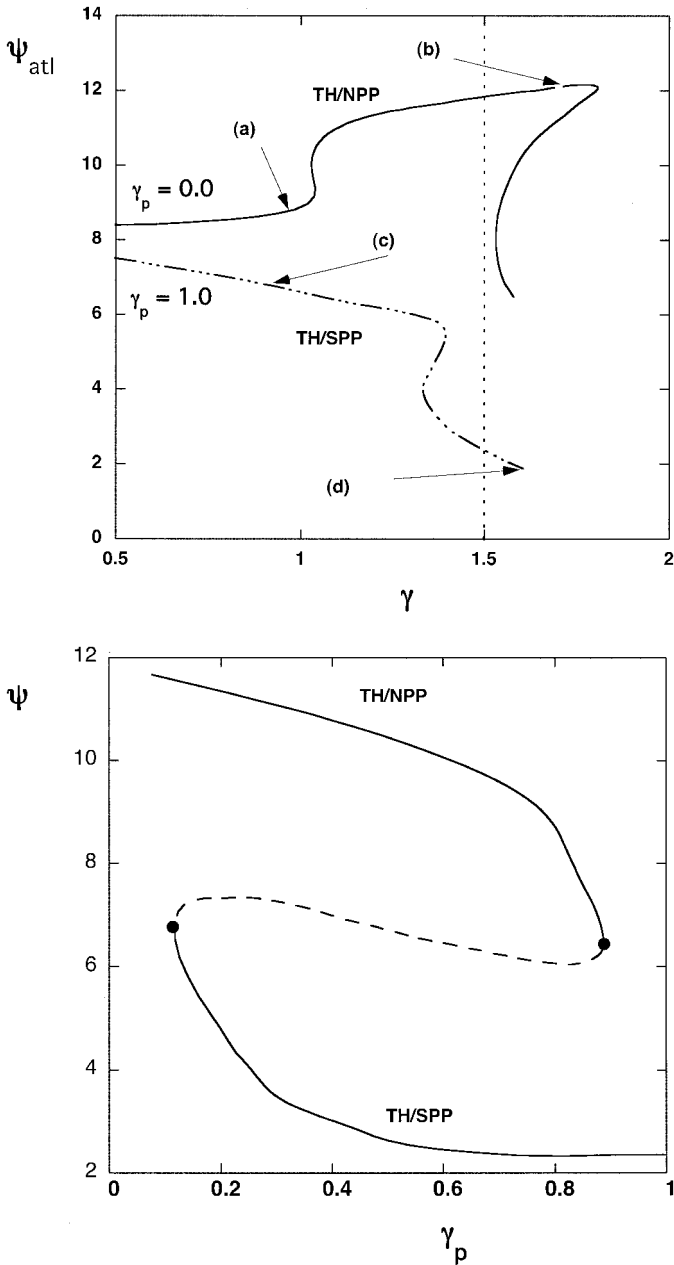


Figure 5. (a) Bifurcation diagrams for two values of γ_p , i.e., $\gamma_p = 0.0$ and $\gamma_p = 1.0$ for $\tau_0 = 0.1$ Pa. Line style does not give indications of stability. (b) Bifurcation diagram with γ_p as control parameter for the case $\gamma = 1.5$ and for $\tau_0 = 0.1$ Pa. Here, drawn curves indicate stable and dashed curves indicate unstable steady states.

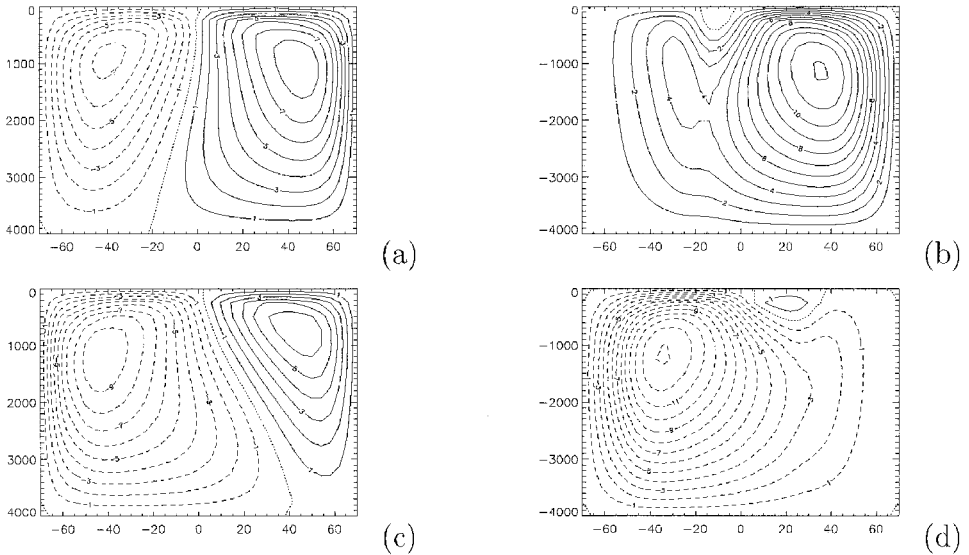


Figure 6. Patterns of the meridional overturning at several labeled locations in Figure 5a. (a) $\gamma = 0.94$, $\Psi_{min} = -7.31$, $\Psi_{max} = 8.70$, (b) $\gamma = 1.69$, $\Psi_{min} = -0.81$, $\Psi_{max} = 12.1$, (c) $\gamma = 0.93$, $\Psi_{min} = -9.79$, $\Psi_{max} = 6.75$ and (d) $\gamma = 1.61$, $\Psi_{min} = -13.1$, $\Psi_{max} = 1.88$. Contour interval is 1 Sv.

salt-advection feedback and the shape of the freshwater flux (as discussed at length in Dijkstra *et al.* (2003)).

When the bifurcation diagram in γ_p is considered for $\gamma = 1.5$ (a value just before the second multiple equilibria regime of the TH/NPP branch), a strong hysteresis loop is found (Fig. 5b). This change in bifurcation diagram with increasing γ_p is qualitatively similar to that in the global ocean model (Fig. 1b). The complication of the small multiple equilibrium regime at larger γ is apparently absent in the global model (it may occur at larger γ). Hence, the results for idealized configuration present a clear view how the hysteresis loop arises. It is through a connection between TH/NPP and TH/SPP branch, which occurs when the freshwater flux shape becomes strongly asymmetric.

4. Dynamics of box models

The first model indicating that multiple equilibria of thermohaline circulation may exist was the Stommel (1961) two-box model. This model consists of an equatorial and a polar box that exchange properties due to a flow whose strength depends on the density difference between the boxes. The density is affected through exchange of salt and heat with the atmosphere above the boxes.

Under conditions that the restoring time scales of heat and salt are different, a typical bifurcation diagram of this model is presented in Figure 7. Here, the dimensionless strength of the circulation Ψ (positive with sinking in the polar box) is plotted versus the

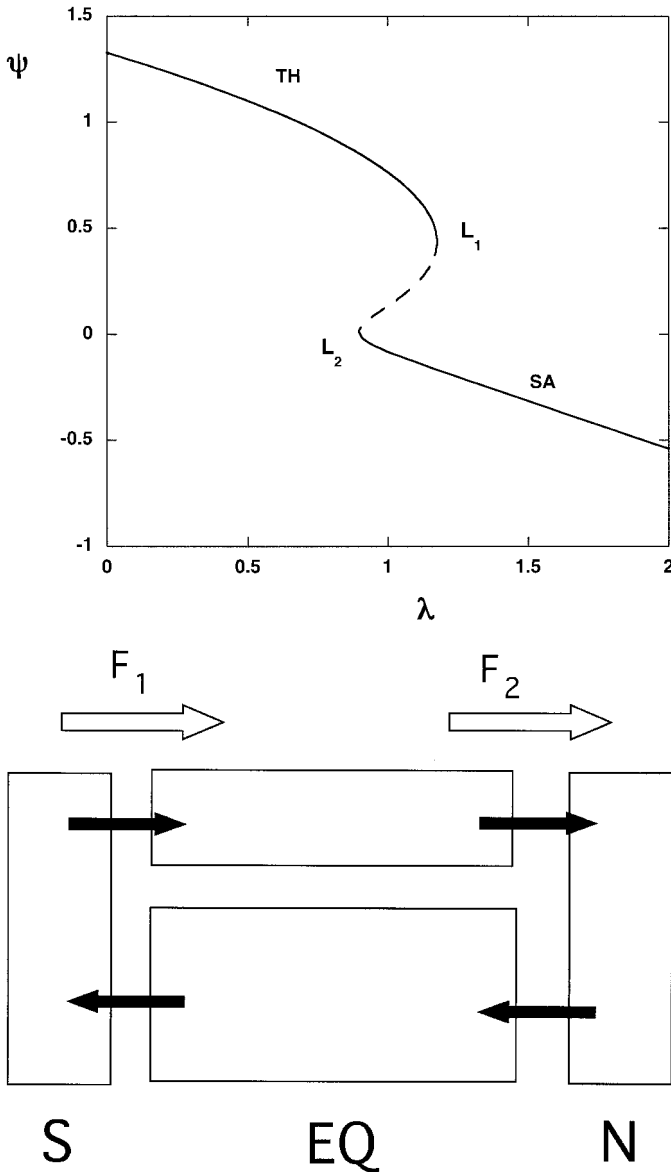


Figure 7. (a) Bifurcation diagram of the Stommel two-box model; in the notation of Chapter 3 in Dijkstra (2000), $\lambda = \eta_2$ is the strength of the freshwater forcing, $\eta_1 = 3.0$ is the strength of the thermal forcing, $\eta_3 = 0.3$ is the ratio of restoring time scales of temperature and salinity, while Ψ is the dimensionless overturning that is proportional to the density difference between the boxes. (b) Sketch of the asymmetrically forced three-box model as in Rahmstorf (1996), with F_1 and F_2 being different freshwater fluxes.

dimensionless strength of the freshwater flux λ . Multiple equilibria occur in the parameter regime between both saddle-node bifurcations L_1 and L_2 . The surface equatorial-to-pole surface circulation, usually referred to as the TH state, can become coexistent with the opposite circulation (the SA state). Transitions between the TH and SA states can occur due to salinity perturbations. The reason is the salt-advection feedback: a positive salinity perturbation in the equatorial box reduces the circulation and consequently the northward salt transport. In this way, less salt enters the polar box and the perturbation is amplified.

The Stommel two-box model cannot be representative for the flow over the total Atlantic with a near-equatorial symmetric surface buoyancy forcing. At least an additional southern box has to be added. Under equatorially symmetric forcing conditions, the TH state in this model is equatorially symmetric, similar as in two back-to-back Stommel two-box models (Welander, 1986). The SA state is also equatorially symmetric with sinking at the equator. Clearly, these flows are not asymmetric pole-to-pole flows with a strong interhemispheric flow. The latter can arise through two mechanisms: spontaneous symmetry breaking or asymmetry in the forcing.

In the three-box model of Rooth (1982), it is assumed that the strength of the Atlantic thermohaline forcing is determined by the north-south density difference between both polar boxes. Although the dynamics of the flow does not differ from that of the Stommel model (Rahmstorf, 1996), equatorially symmetric solutions are excluded because there can be no upwelling in the equatorial box. It turns out that the strength of the overturning in this model indeed increases with increasing freshwater forcing since in this model, the salinity gradient is such that it stimulates the flow, making it fundamentally different from the single-hemispheric cases. Through exclusion of equatorially symmetric solutions, the interhemispheric transport is totally attributed to asymmetric (external) factors.

If in the Welander (1986) model, where the flow strength is related to the equator-pole density difference, the stability of the TH flow is considered an important feature: the TH solution is unstable to equatorially asymmetric perturbations. This leads to the appearance of symmetry breaking pitchfork bifurcations. As a consequence of this spontaneous symmetry breaking, asymmetric pole-to-pole flows appear. A typical bifurcation of the three-box model is plotted in Figure 8a (Thual and McWilliams, 1992). The TH and SA solution branches in this diagram are similar to those in the back-to-back Stommel model, while the NPP and SPP pole-to-pole solution branches are additional. Hence, asymmetric circulations arise spontaneously through the salt-advection feedback. For such an asymmetric solution, this feedback contributes to the overturning strength of the circulation. Hence, an increase in the gradient of the freshwater flux does not brake the circulation but enhances it.

When external equatorial asymmetry is added to the Welander (1986) model, the pitchfork bifurcations in Figure 8a disappear and a so-called imperfection occurs. A typical bifurcation diagram, which may occur if the temperature forcing in the northern box is made stronger than in the southern box, is plotted in Figure 8b. Here, the connection

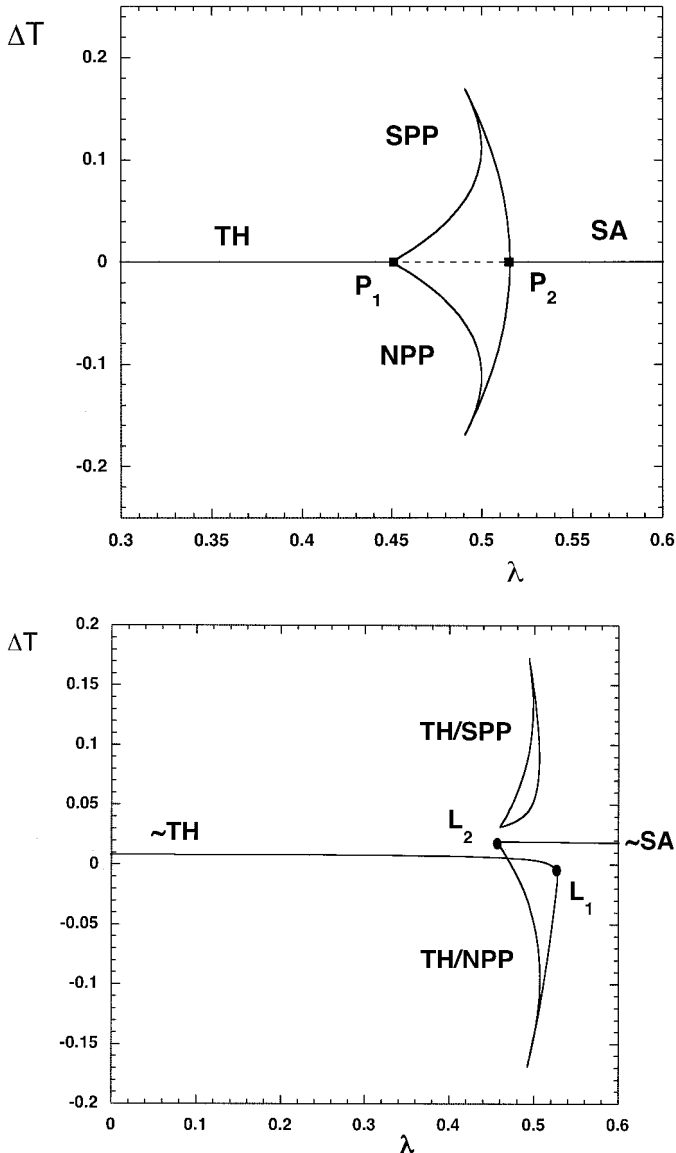


Figure 8. (a) Bifurcation diagram of the back-to-back Stommel three-box model (Welander, 1986); in the notation of Chapter 3 in Dijkstra (2000), λ is the dimensionless freshwater-flux strength and ΔT is the north-south temperature difference. (b) Bifurcation diagram of a typical asymmetrically forced situation in the three-box model (an imperfection).

between the TH and SPP solution becomes an isolated branch while the TH/NPP branch exists for all λ . When the asymmetry is increased, the TH/SPP solution eventually disappears.

Comparison of the bifurcation diagrams between the box models and the Atlantic model (and hence the global model) provides the following insight. The asymmetric solutions that appear due to symmetry breaking in the Welander (1986) model are the ones that correspond most to that of the Atlantic-only model with near-equatorial forcing. However, the degree to which external asymmetry affects the different branches determines whether the fully asymmetric case as represented in the Rooth (1982) model applies. If the asymmetry is totally dominating, then the Rooth (1982) model is adequate, whereas if the asymmetry is not strong enough, then isolated solution branches may be present which the Rooth (1982) model cannot represent.

5. Summary and discussion

Having computed bifurcation diagrams for a hierarchy of models of the thermohaline circulation, we are now in a position to give a definite answer to the problem posed in the introduction: *the hysteresis diagram of the global ocean circulation arises through a connection of the TH/NPP and TH/SPP branches once the freshwater flux becomes strongly asymmetric.*

The relevant situation in understanding the origin of the hysteresis in the global model is the equatorially symmetric double-hemispheric problem. In the Welander three-box model (Welander, 1986; Thual and McWilliams, 1992), in two-dimensional Boussinesq models (Cessi and Young, 1992; Quon and Ghil, 1992; Dijkstra and Molemaker, 1997) and in single-basin zonally averaged models (Wright and Stocker, 1991), a pitchfork bifurcation exists (Vellinga, 1996). Hence, the NPP and SPP solutions arise through symmetry breaking and the important characteristic of these solutions is that the salt-advection feedback is active in maintaining the circulation. Hence, the overturning increases with increasing strength of the equatorially symmetric freshwater flux (Dijkstra and Molemaker, 1997). The same pitchfork bifurcation is also found in equatorially symmetric three-dimensional double hemispheric configurations (Weijer and Dijkstra, 2001).

The character of the pitchfork, being either subcritical or supercritical, depends on the shape of the freshwater flux. With a zonally averaged representation of this flux, which takes the equatorial precipitation regions into account, the pitchfork turns out to be subcritical and leads, for the southern sinking as well as for the northern sinking solutions, to (an interval of) small hysteresis behavior. This is an additional source of multiple equilibria, besides the coexistence of the NPP and SPP states. It leads to the existence of just stronger and weaker overturning states; the difference in meridional overturning is just a few Sverdrup (Dijkstra *et al.*, 2003).

The degree of asymmetry of forcing and boundary conditions (continental geometry) subsequently becomes central to the location of the different equilibria in parameter space. As soon as asymmetry is present, the pitchfork bifurcation ceases to exist and isolated branches may appear. The dominant asymmetries in the real Atlantic Ocean and their effect on the solution branches is summarized as follows.

- The present surface freshwater flux appears to be slightly asymmetric. When the zonally averaged profile for the Atlantic is considered (Oberhuber, 1988; Zaucker *et al.*, 1994), there is slightly more net evaporation in the northern part than in the southern part of the basin. This certainly favors the northern sinking branch.
- The continental geometry of the Atlantic is quite asymmetric, with the northern basin closing toward the north and the southern basin opening toward the south. The area of ocean-atmosphere interaction, therefore, considerably changes in meridional direction and this has consequences for the strength of the atmospheric feedback on sea-surface temperature anomalies (Marotzke and Stone, 1995; Dijkstra and Neelin, 2000). Within a two-dimensional model, this asymmetry induces a preference for the northern sinking branch. The TH/SPP branch disappears through the combination of both continental asymmetry and asymmetry in the freshwater flux (Dijkstra and Neelin, 2000) by shifting out of the realistic domain.
- The salt and heat input into the Atlantic basin due to inter-basin exchanges is strongly asymmetric. In the northern hemisphere, an important component of this inflow comes from the Mediterranean and the Arctic oceans. Compensation (Gordon, 1986; Schmitz, 1995) of the outflow of North Atlantic Deep Water is accomplished through water coming from the Indian Ocean (the ‘warm’ water path) and that coming through Drake Passage (the ‘cold’ water path). Both compensation routes provide a complicated structure of heat and salt input into the South Atlantic (Weijer *et al.*, 2001). Strong preferences for some of the equilibria may occur since one of the disconnected branches of solutions moves out of the ‘realistic’ range of parameter space or disappears through an isola (Weijer *et al.*, 1999, 2001).
- The opening in the Southern Ocean impedes meridional flow since there is no topography to support meridional flow above the sill depth of Drake Passage. Moreover, a strong Antarctic Circumpolar Current (ACC) is present at the southern part of the basin and absent in the north. The presence of such a current influences the structure of the density field which may influence the equilibria in the Atlantic basin (Toggweiler and Samuels, 1995). As was shown here for the Atlantic model, the effect of the southern opening shows a strong asymmetry and deforms the TH/SPP branch into an isolated closed branch. This branch remains existent in the absence of the zonally averaged wind under an equatorially symmetric freshwater flux.
- The winds over the Atlantic are fairly asymmetric about the equator. From the zonally averaged wind-stress shape, one observes that the winds over the Southern Ocean are much stronger than those over the rest of the basin (Rahmstorf and England, 1997). The TH/SPP branch in the Atlantic model disappears when the wind-stress forcing is included (Dijkstra *et al.*, 2003) leaving a single branch of northern sinking solutions. This is caused by the Ekman flow in the Southern Ocean, which restricts the domain of existence of the southern sinking solution.

The input of a regional freshwater perturbation flux, here represented by γ_p , forms an additional parameter controlling asymmetry of the system. When wind-stress forcing is

considered and slices are made in γ for fixed values of γ_p , one sees a transition from a bifurcation diagram with only the TH/NPP branch (at small γ_p) to a single branch with only the TH/SPP branch (at large γ_p). In the latter case, the asymmetry due to the additional freshwater flux is so strong that it opposes and overrules the preference of the northern sinking solution due to the southern channel and winds.

Therefore, when the variations of the equilibria in γ_p for fixed γ are considered, one smoothly connects the TH/NPP branch with the TH/SPP branch. This creates a large hysteresis between northern sinking and southern sinking solutions. Although this appears like a Stommel type bifurcation diagram, it is essentially different because the salt-advection feedback maintains both TH/NPP and TH/SPP states. In the limit that asymmetry is so strong that there are no isolated solution branches, the Rooth (1982) model is a correct dynamical model. In other cases, the asymmetric Welander (1986) model is a better prototype for the dynamics. Both models predict an increase (with γ) in northern overturning on the TH/NPP branch and southern overturning on the TH/SPP branch.

In conclusion, to understand the origin of the hysteresis regime as well as the interhemispheric transport, the studies through the hierarchy of models starting at the double-hemispheric equatorially symmetric situation are very useful. The result is a new conceptual view on the mechanisms controlling the transitions between northern and southern sinking states. The latter may have been at the heart of climate variability in the geological past.

Acknowledgments. This work was supported by the Netherlands Organization for Scientific Research (N.W.O.) under a PIONIER grant to the first author. Use of the computing facilities was sponsored by the National Computing Facilities Foundation (N.C.F.) within the project SG029 with financial support from N.W.O.

REFERENCES

- Bryan, F. O. 1986. High-latitude salinity effects and interhemispheric thermohaline circulations. *Nature*, *323*, 301–304.
- Cessi, P. and W. R. Young. 1992. Multiple equilibria in two-dimensional thermohaline circulation. *J. Fluid Mech.*, *241*, 291–309.
- Dijkstra, H. A. and M. J. Molemaker. 1997. Symmetry breaking and overturning oscillations in thermohaline-driven flows. *J. Fluid Mech.*, *331*, 195–232.
- Dijkstra, H. A. and J. D. Neelin. 2000. Imperfections of the thermohaline circulation: Latitudinal asymmetry versus asymmetric freshwater flux. *J. Climate*, *13*, 366–382.
- Dijkstra, H. A., W. Weijer and J. D. Neelin. 2003. Imperfections of the three-dimensional thermohaline ocean circulation: Hysteresis and unique state regimes. *J. Phys. Oceanogr.* *33*, 2796–2814.
- Ganachaud, A. and C. Wunsch. 2000. Improved estimates of global ocean circulation, heat transport and mixing from hydrographic data. *Nature*, *408*, 453–457.
- Gordon, A. L. 1986. Interocean exchange of thermocline water. *J. Geophys. Res.*, *91*, 5037–5046.
- Josey, S. A., E. C. Kent and P. K. Taylor. 1999. New insights into the ocean heat budget closure problem from analysis of the SOC air-sea flux climatology. *J. Climate*, *12*, 2856–2880.
- Levitus, S., R. Burgett and T. Boyer. 1994. World Ocean Atlas 1994, 3: Salinity. NOAA Atlas NESDIS 3, US Department of Commerce, Washington DC; 0–99.

- Marotzke, J. 2000. Abrupt climate change and thermohaline circulation: Mechanisms and predictability. *Proc. Natl. Acad. Sci.*, *97*, 1347–1350.
- Marotzke, J. and P. Stone. 1995. Atmospheric transports, the thermohaline circulation and flux adjustments in a simple coupled model. *J. Phys. Oceanogr.*, *25*, 1350–1364.
- Oberhuber, J. M. 1988. The Budget of Heat, Buoyancy and Turbulent Kinetic Energy at the Surface of the Global Ocean. Max Planck Institute für Meteorologie Hamburg Report No. 15, Hamburg, Germany.
- Prange, M., V. Romanova and G. Lohmann. 2002. The glacial thermohaline circulation: stable or unstable? *Geophys. Res. Lett.*, *29*, (21), 2028, doi: 10.1029/2002GLO15337, 24-1-24-4.
- Quon, C. and M. Ghil. 1992. Multiple equilibria in thermohaline convection due to salt-flux boundary conditions. *J. Fluid Mech.*, *245*, 449–484.
- Rahmstorf, S. 1995. Bifurcations of the Atlantic thermohaline circulation in response to changes in the hydrological cycle. *Nature*, *378*, 145–149.
- 1996. On the freshwater forcing and transport of the Atlantic thermohaline circulation. *Climate Dyn.*, *12*, 799–811.
- 2000. The thermohaline circulation: a system with dangerous thresholds? *Climatic Change*, *46*, 247–256.
- 2003. The current climate. *Nature*, *421*, 699.
- Rahmstorf, S. and M. England. 1997. Influence of Southern Hemisphere winds on North Atlantic deep water flow. *J. Phys. Oceanogr.*, *27*, 2040–2054.
- Rooth, C. 1982. Hydrology and ocean circulation. *Progr. Oceanogr.*, *11*, 131–149.
- Schmitz, W. J. 1995. On the interbasin-scale thermohaline circulation. *Rev. Geophys.*, *33*, 151–173.
- Stommel, H. 1961. Thermohaline convection with two stable regimes of flow. *Tellus*, *13*, 224–230.
- Thual, O. and J. C. McWilliams. 1992. The catastrophe structure of thermohaline convection in a two-dimensional fluid model and a comparison with low-order box models. *Geophys. Astrophys. Fluid Dyn.*, *64*, 67–95.
- Toggweiler, J. R. and B. Samuels. 1995. Effect of Drake Passage on the global thermohaline circulation. *Deep-Sea Res.*, *42*, 477–500.
- Trenberth, K. E., J. G. Olson and W. G. Large. 1989. A global ocean wind stress climatology based on ECMWF analyses. Technical report, National Center for Atmospheric Research, Boulder, CO, U.S.A.
- Vellinga, M. 1996. Instability of two-dimensional thermohaline circulation. *J. Phys. Oceanogr.*, *26*, 305–319.
- Weaver, A. J. and T. M. Hughes. 1996. On the incompatibility of ocean and atmosphere and the need for flux adjustments. *Climate Dyn.*, *12*, 141–170.
- Weijer, W., W. De Ruijter and H. A. Dijkstra. 2001. Stability of the Atlantic overturning circulation: competition between Bering Strait freshwater flux and Agulhas heat and salt sources. *J. Phys. Oceanogr.*, *31*, 2385–2402.
- Weijer, W., W. P. M. De Ruijter, H. A. Dijkstra and P. J. Van Leeuwen. 1999. Impact of interbasin exchange on the Atlantic overturning circulation. *J. Phys. Oceanogr.*, *29*, 2266–2284.
- Weijer, W. and H. A. Dijkstra. 2001. Bifurcations of the three-dimensional thermohaline circulation: The double hemispheric case. *J. Mar. Res.*, *59*, 599–631.
- 2003. Stability of the global ocean circulation: basic bifurcation diagrams. *J. Phys. Oceanogr.* (submitted).
- Welander, P. 1986. Thermohaline effects in the ocean circulation and related simple models, *in* Large-Scale Transport Processes in Oceans and Atmosphere, J. Willebrand and D. L. T. Anderson, eds., D. Reidel, 163–200.

- Wright, D. G. and T. F. Stocker. 1991. A zonally averaged model for the thermohaline circulation, Part I: Model development and flow dynamics. *J. Phys. Oceanogr.*, *21*, 1713–1724.
- Wunsch, C. 2002. What is the thermohaline circulation? *Science*, *298*, 1179–1180.
- Zaucker, F., T. F. Stocker and W. S. Broecker. 1994. Atmospheric freshwater fluxes and their effect on the global thermohaline circulation. *J. Geophys. Res.*, *99*, 12,443–12,457.

Received: *16 June, 2003*; revised: *12 November, 2003*.